PTEP

Prog. Theor. Exp. Phys. **2016**, 091D01 (9 pages)
DOI: 10.1093/ptep/ptw130

Letter

First application of superconducting transition-edge sensor microcalorimeters to hadronic atom X-ray spectroscopy

HEATES Collaboration

S. Okada[†,1,*], D. A. Bennett[2], C. Curceanu[3], W. B. Doriese[2], J. W. Fowler[2], J. D. Gard[2], F. P. Gustafsson[4], T. Hashimoto[1], R. S. Hayano[5], S. Hirenzaki[6], J. P. Hays-Wehle[2], G. C. Hilton[2], N. Ikeno[7], M. Iliescu[3], S. Ishimoto[8], K. Itahashi[1], M. Iwasaki[1], T. Koike[9], K. Kuwabara[10], Y. Ma[1], J. Marton[11], H. Noda[‡,1], G. C. O'Neil[2], H. Outa[1], C. D. Reintsema[2], M. Sato[1], D. R. Schmidt[2], H. Shi[3], K. Suzuki[11], T. Suzuki[5], D. S. Swetz[2], H. Tatsuno[§,8,2], J. Uhlig[4], J. N. Ullom[2], E. Widmann[11], S. Yamada[10], J. Yamagata-Sekihara[12], and J. Zmeskal[11]

[1]*RIKEN Nishina Center, RIKEN, Wako 351-0198, Japan*
[2]*National Institute of Standards and Technology, Boulder, CO 80305, USA*
[3]*Laboratori Nazionali di Frascati dell' INFN, I-00044 Frascati, Italy*
[4]*Lund University, Box 117, 221 00 Lund, Sweden*
[5]*Department of Physics, The University of Tokyo, Tokyo 113-0033, Japan*
[6]*Department of Physics, Nara Women's University, Kita-Uoya Nishimachi, Nara 630-8506, Japan*
[7]*Department of Regional Environment, Tottori University, Tottori 680-8551, Japan*
[8]*High Energy Accelerator Research Organization, KEK, Tsukuba 305-0801, Japan*
[9]*Research Center for Physics and Mathematics, Osaka Electro-Communication University, Neyagawa, Osaka 572-8530, Japan*
[10]*Tokyo Metropolitan University, Hachioji 192-0397, Japan*
[11]*Stefan-Meyer-Institut für Subatomare Physik, A-1090 Vienna, Austria*
[12]*National Institute of Technology, Oshima College, Oshima, Yamaguchi 742-2193, Japan*
[†]*Present address: AMO Physics Laboratory, RIKEN, Wako 351-0198, Japan*
[‡]*Present address: Frontier Research Institute for Interdisciplinary Sciences, Tohoku University, Sendai 980-8578, Japan*
[§]*Present address: Lund University, Box 117, 221 00 Lund, Sweden*
[*]E-mail: sokada@riken.jp

Received July 21, 2016; Revised August 10, 2016; Accepted August 16, 2016; Published September 30, 2016

High-resolution pionic atom X-ray spectroscopy was performed with an X-ray spectrometer based on a 240 pixel array of superconducting transition-edge sensor (TES) microcalorimeters at the πM1 beam line of the Paul Scherrer Institute. X-rays emitted by pionic carbon via the $4f \rightarrow 3d$ transition and the parallel $4d \rightarrow 3p$ transition were observed with a full width at half maximum energy resolution of 6.8 eV at 6.4 keV. The measured X-ray energies are consistent with calculated electromagnetic values which considered the strong interaction effect assessed via the Seki–Masutani potential for the $3p$ energy level, and favor the electronic population of two filled $1s$ electrons in the K-shell. Absolute energy calibration with an uncertainty of 0.1 eV was demonstrated under a high-rate hadron beam condition of 1.45 MHz. This is the first application of a TES spectrometer to hadronic atom X-ray spectroscopy and is an important milestone towards next-generation high-resolution kaonic atom X-ray spectroscopy.

Subject Index D01, D15, D33, H13, H15

1. *Introduction* A hadronic atom consists of a negatively charged hadron (e.g., π^-, K^-, $\bar{p}$, Σ^-, Ξ^-) and electrons that are bound by a Coulomb field to an atomic nucleus. Such a system can be used to probe the strong interaction between hadrons and atomic nuclei in the low-energy limit. The mass of the hadron, significantly larger than the mass of the electron it replaces, shifts the atomic transition energies in the hadronic atom to significantly higher energies than those of the standard atom. In addition, effects of the strong interaction appear in the most tightly bound energy level. These perturbations include an energy shift from that given only by the electromagnetic interaction, and a lifetime broadening due to absorption of the hadron by the nucleus. The shift and width can be experimentally extracted via X-ray emission spectroscopy of characteristic transitions into this lowest orbital.

In kaonic atoms, the understanding of the low-energy $\overline{K}N$ interaction has been substantially deepened by the most recent kaonic hydrogen atom measurement [1,2] and theoretical studies (e.g., [3,4]). However, the depth of the $\overline{K}$-nucleus potential remains unknown because of insufficient precision in the kaonic atom data for $Z \geq 2$; this is one of the greatest present concerns in strangeness nuclear physics [5].

In recent years, Balmer-series X-rays of the K^--He atom ($\sim$6 keV) were measured at the K5 beamline of KEK-PS [6] and the DAΦNE electron–positron collider of the Laboratori Nazionali di Frascati [7,8]. These measurements followed discussions of the importance of the measurement of the strong interaction shift and width of the $2p$ level in kaonic helium atoms (K^--He) over 30 years ago [9,10]. Both experiments employed silicon drift detectors (SDDs) whose full width at half maximum (FWHM) energy resolution is typically $\sim$200 eV at 6 keV [6–8]. To observe spectral effects as predicted by theoretical calculations [11–13], e.g., a 0.2 eV shift and 2 eV line width, a new approach with a significantly improved resolution is essential.

We are preparing a high-resolution X-ray measurement of kaonic atoms at a kaon beamline of J-PARC [14] using a novel superconducting transition-edge sensor (TES) microcalorimeter (J-PARC E62 [15]). The FWHM energy resolution of this type of detector can be as good as about 2 eV at 6 keV [16,17], which is about two orders of magnitude better than that of SDDs. The spectrometer is a highly sensitive thermal sensor that measures energy deposition via the increase in the resistance of a superconducting thin film that is biased within the sharp phase transition between the normal and superconducting phases. The detailed working principles and the recent progress of the TES system are described in Refs. [17–19].

An alternate high-resolution X-ray spectroscopy technology is based on diffraction from Bragg crystals. However, they have not been used to study the strong interaction in most hadronic atoms due to their low efficiency. Only pion beams and the resulting X-ray emission are intense enough to enable the study of pionic atom X-rays [20,21] with crystal spectrometers. On the other hand, recent technological advances in multiplexed readout of multi-pixel TES arrays (more than 100 pixels, each having $\sim$0.1 mm^2 effective area) allow the performance of a precision kaonic atom measurement in a realistic data acquisition time.

Until this experiment, a TES X-ray spectrometer has never been utilized in a hadron beam environment. To study the in-beam performance of the TES spectrometer at a hadron beamline and demonstrate the feasibility of TES-based hadronic atom X-ray spectroscopy, we performed a pioneering experiment at a pion beamline by measuring the X-rays from the $4f \rightarrow 3d$ transition of pionic carbon (π-^{12}C). This X-ray transition was chosen because the energy ($\sim$6.5 keV) is similar to the K^--He $3 \rightarrow 2$ X-ray energy, while the strong interaction effects are negligibly small.

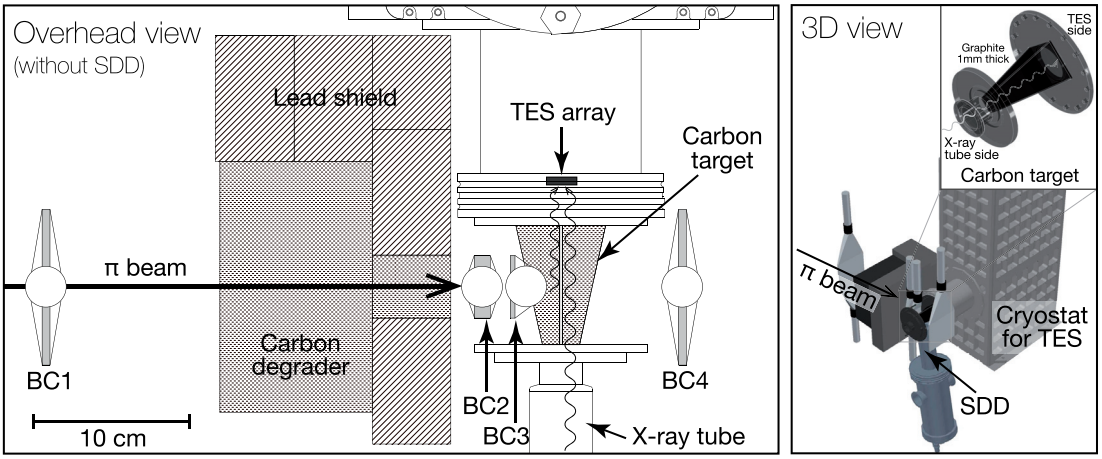

Fig. 1. A top view (left) and birds-eye view (right) of the experimental setup.

2. *Experiment* The experiment was carried out at the πM1 beamline [22] of the Paul Scherrer Institute (PSI) in October 2014. Pions were created by a proton beam of energy 590 MeV at a current of up to 2.3 mA passing through a graphite target located in the main beamline of the PSI synchro-cyclotron, and were transported through the πM1 beamline.

A schematic view of the experimental setup is shown in Fig. 1. With a 2.2 mA primary proton beam, the π^- beam rate with momentum 173 MeV/c was $1.45 \times 10^6\,\mathrm{s}^{-1}$ at BC1 ($10 \times 10\,\mathrm{cm}^2$ plastic scintillation counter) located at a distance 30 cm upstream from the focal point. The π^-/e^- ratio was $\sim$0.7 due to a missing electrostatic separator in the beamline.

The incident π^-s were degraded in moderators, counted with beamline counters (BCs), and stopped in a carbon graphite target where π-^{12}C atoms were generated. X-rays were emitted by the highly excited atoms and detected by a TES X-ray spectrometer through a 150 μm-thick beryllium vacuum window and three layers of 5 μm-thick aluminum IR-blocking filters (one at each of the three temperature stages: 50 K, 3 K, 50 mK).

A 240 pixel TES array [23] was the X-ray spectrometer. Each pixel had a 4 μm-thick bismuth absorber (80% absorption efficiency for 6.4 keV X-rays) which converted the incident X-ray energy to heat; the absorber was coupled to a sensitive thermal sensor, the TES, composed of a superconducting Mo/Cu proximity bilayer film. Each absorber had a collimated effective area of 320 μm $\times$ 305 μm, and thus the total collecting area of the array was about 23 mm^2. Each TES pixel was electrically biased to the superconducting critical temperature ($T_\mathrm{C} \sim 107$ mK) and to about 20%–30% of their normal resistance of $\sim$10 mΩ. A pulse-tube-backed adiabatic demagnetization refrigerator (ADR) [24] cooled the system to a regulated bath temperature of 75 mK $\pm$ 7 μK (rms). The regulated hold time was about 36 hours, after which the ADR cycle (magnetic field increased isothermally and decreased adiabatically) took 2 hours before another 36 hours of operation at 75 mK.

SQUID current amplifiers were used to read out the current signal from the low-resistance TESs. For the 240 pixel readout, a time division SQUID multiplexing (TDM) scheme [25] was employed to reduce the number of wires running to the low-temperature stages of the cryocooler. The signal from each TES channel was coupled to a SQUID amplifier, and the outputs from 30 individual channels were switched sequentially and read out by a single amplifier. The multiplexing frame time was 9.6 μs (0.32 μs/channel). The sampling rate was therefore 104 kHz for each pixel. The 240 pixel readout was realized by using eight TDM columns in parallel.

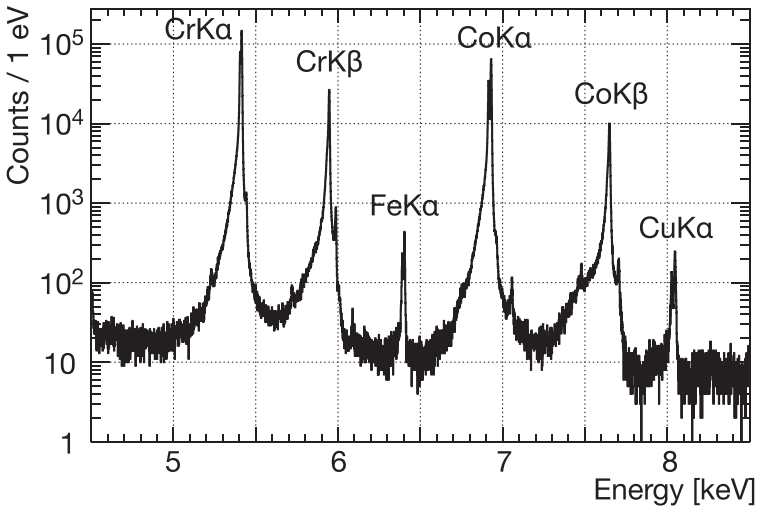

Fig. 2. An X-ray energy spectrum obtained from a tube source X-ray generator shining on Cr and Co calibration pieces without a pion beam. The Cr K_α, Cr K_β, Co K_α, and Co K_β lines are used for the energy calibration. Lower-yield X-rays, Fe K_α (6.4 keV) and Cu K_α (8.0 keV), originate respectively from the stainless steel vacuum fittings of the tube source and the metal structure of the 50 mK detector package.

TES data were continuously streamed into a PC server, and were recorded to disk only when a current "pulse" due to an X-ray event was triggered. The system recorded 1024 samples (9.83 ms) for each event, where the first 256 samples corresponded to a pre-triggered timing region. The typical exponential rise and decay time constants of an X-ray pulse were $\sim$200 μsec and $\sim$500 μsec respectively. The X-ray energy corresponding to each pulse height was calculated with an optimal filter technique [26]. The data acquisition system also recorded a stopped-π trigger timing defined by beamline counters as BC1 $\otimes$ BC2 $\otimes$ BC3 $\otimes$ $\overline{\text{BC4}}$, where the pulse height threshold of BC2 was carefully set in order to select only stopped-pion events which deposited more energy than an electron, a muon, or an in-flight pion event. The relative timing of this triggering system to the TES events was reconstructed during the offline analysis.

Precise absolute energy calibration was crucial for this measurement. Because independent energy calibration was necessary for each of the 240 pixels, it was essential to supply intense calibration X-rays to achieve sufficient statistics for *in situ* calibration. An X-ray tube source was installed as shown in Fig. 1. Characteristic X-rays were produced by shining a controllable flux of X-rays, which was generated by an electron gun with a Rh target, on 99.999% pure chromium and cobalt pieces. These calibration X-rays traveled through the hollow, conical carbon target to the TES spectrometers.

Figure 2 shows a summed X-ray energy spectrum of 209 working TES pixels obtained with the X-ray generator without a pion beam. The achieved energy resolution was 4.6 eV (FWHM) at 6.4 keV with a count rate of 4.4 Hz/pixel. The energy calibration was performed with the four calibration X-ray lines Cr K_α, Cr K_β, Co K_α, and Co K_β, with natural cubic spline interpolation. The energies and natural widths of the calibration X-rays were fixed with the reference values [27] in the spectral fitting. Lower-yield X-rays, Fe K_α (6.4 keV) and Cu K_α (8.0 keV), originated respectively from stainless steel vacuum fittings in the tube source and Cu inside of the detector package. These were not used for calibration.

3. *Results* Time and energy distributions of π-^{12}C X-rays measured with the 209 working TES pixels are shown in Fig. 3. The data were accumulated for 13.5 hours with a pion beam intensity of 1.45 MHz and a stopped-π trigger rate of 34.5 kHz. Figure 3(b) shows a distribution of the time difference between pion arrival and X-ray detection with the TES array for stopped-π^- trigger events. A clear peak was observed with a time resolution of 1.2 μsec FWHM. Figure 3(a) shows a correlation plot of the time difference versus the X-ray energy measured by TESs. At around 6.43 keV, a clear time–energy correlation corresponding to π-^{12}C $4f \rightarrow 3d$ X-rays was observed. Figure 3(c) shows an X-ray energy spectrum of only those events recorded within the stopped-π^- timing gate ($\pm$1.5 μsec) that is indicated in Fig. 3(b). A sharp peak from the π-^{12}C $4f \rightarrow 3d$ transition is observed. The TES spectrometer has sufficient energy resolution to observe the parallel transition $4d \rightarrow 3p$. Figure 3(c) shows contributions from those $4f \rightarrow 3d$ and $4d \rightarrow 3p$ lines, whose centroids are only 7.4 eV apart. The timing selection improved the peak-to-background ratio of the π-^{12}C line from 2 to 10. As a reference in this experiment, an SDD is installed just beneath the carbon target as shown in the right panel of Fig. 1. The FWHM energy resolution of the SDD of $\sim$165 eV is not nearly enough to resolve any of the important features of the spectrum [Fig. 3(d)].

The tube source produces Cr and Co calibration X-rays constantly during data acquisition with the pion beam. The energy calibration with Cr and Co X-rays is recalculated every 2 hours to mitigate gain drift. A fit of the energy spectrum with the in-beam condition of the π^- beam gives an FWHM energy resolution of 6.8 eV at 6.4 keV with a TES hit rate of 4.8 Hz/pixel, of which 0.4 Hz is due to the pion beam. The deterioration of the energy resolution and the size of low-energy and high-energy tail components in the non-Gaussian energy response of TESs both increase as a function of pion beam intensity. These beam-correlated effects are explained by the production of thermal cross-talk pulses which are due to direct charged particle hits in the silicon substrate of the TES array. The detail of the detector response and the absolute energy calibration was presented in a separate paper [28].

The X-ray generator fluoresces materials containing iron (e.g., the stainless steel vacuum fittings around the target cell); therefore, characteristic X-rays of iron are observed that are uncorrelated with the pion beam timing. The Fe $K_{\alpha 1}$ (6.404 keV) and Fe $K_{\alpha 2}$ (6.391 keV) lines were used to evaluate the accuracy of the energy calibration that was then used to determine the π-^{12}C X-ray energy. A result of a spectral fit of Fe K_α and π-^{12}C X-rays is shown in Fig. 3(c). The energy calibration accuracy is assessed by the fit to the measured Fe K_α line. The measured energy of our Fe $K_{\alpha 11}$ line is

$$6404.07 \pm 0.10(\text{stat.})^{+0.06}_{-0.04}(\text{syst.})\ \text{eV},$$

where the first error is statistical and the second is systematic. The quoted systematic uncertainty is a quadratic summation of the contributions from the continuum background parameter and the asymmetry of the fit function. A comparison with the reference value of 6404.148(2) eV [27] for pure, metallic iron shows good agreement within the errors. To determine the energy of pionic carbon transition X-rays, the critical issue is the uncertainty precisely at the lines of interest, 6430 eV. It is difficult to assess the systematic uncertainty introduced by our choice for the calibration curves in its full generality. Fortunately, the Fe K_α line at 6404 eV is very close to the line of interest, and this good agreement with the reference value validated the choice of the present energy calibration curves.

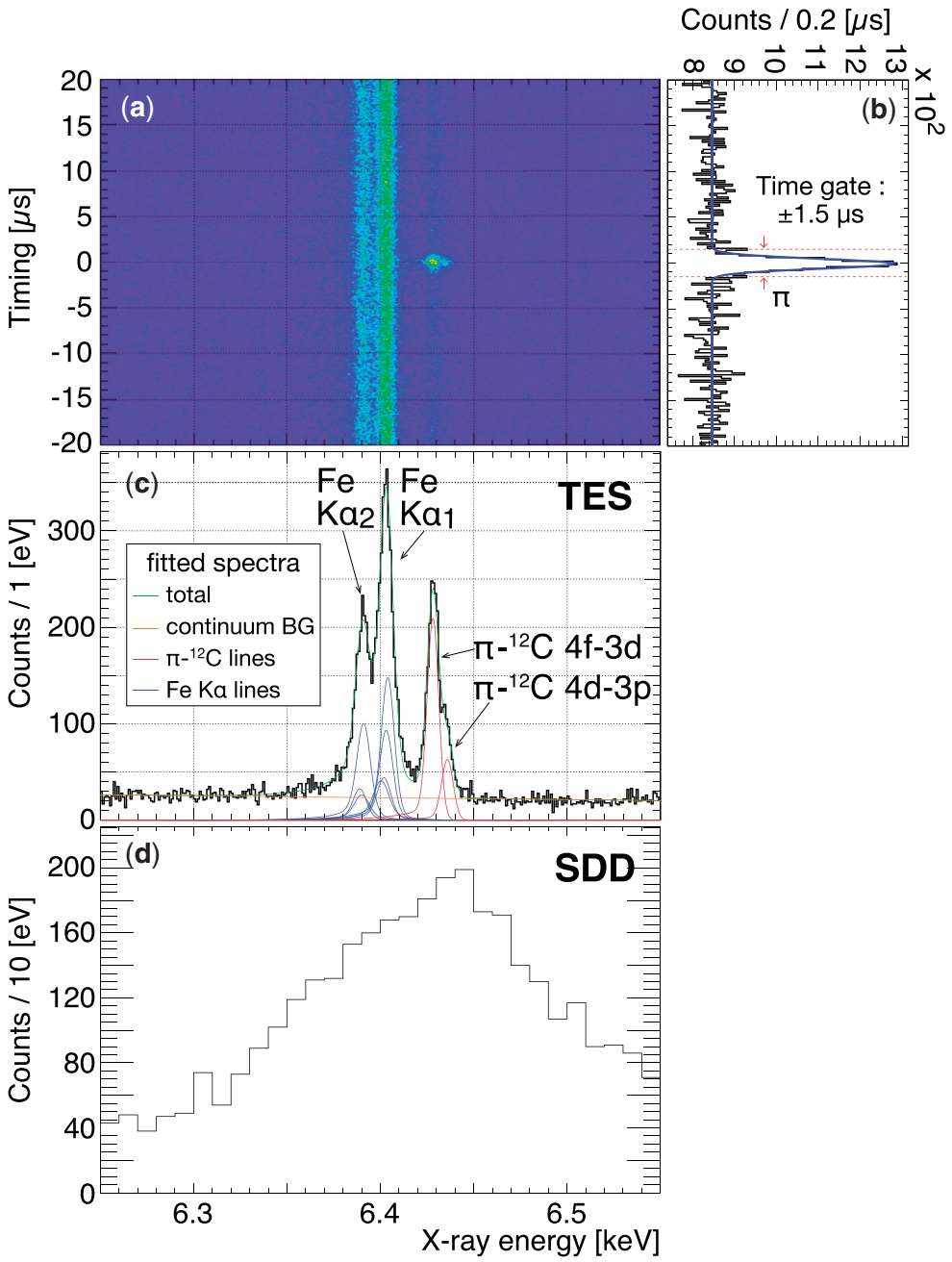

Fig. 3. Results of the measured X-ray time and energy distributions for stopped-π^- trigger events. (a) A correlation plot of the time difference between pion arrival and X-ray detection vs the X-ray energy measured by the TES array. (b) The projection on the time axis showing timing resolution of 1.2 μs (FWHM). A time gate of ± 1.5 μs is used in the analysis. (c) The projection on the energy axis by selecting the stopped-π^- time gate indicated in (b), where the fitted components for Fe K_α and π-^{12}C X-rays are also shown. (d) The same spectrum measured by the reference SDD having an FWHM energy resolution of $\sim$165 eV.

Fits to our energy spectra determined the energies of the π-^{12}C $4f \rightarrow 3d$ and $4d \rightarrow 3p$ transition X-rays and their yield ratios to be:

$$E(4f \rightarrow 3d) = 6428.39 \pm 0.13(\text{stat.}) \pm 0.09(\text{syst.}) \text{ eV},$$
$$E(4d \rightarrow 3p) = 6435.76 \pm 0.30(\text{stat.})^{+0.11}_{-0.07}(\text{syst.}) \text{ eV},$$

Table 1. Calculated values of pionic ^{12}C electromagnetic energies and strong interaction energy shifts via the Seki–Masutani potential [30]. For the $4f \rightarrow 3d$ and $4d \rightarrow 3p$ transitions, electron screening effects are assessed with the cases of filling one $1s$ electron and two $1s$ electrons in the K-shell. The experimental results are also shown.

State	K.G. energy (eV)	Vacuum polarization $\alpha(Z\alpha)$ (eV)	Vacuum polarization $\alpha^2(Z\alpha)$ (eV)	Nuclear finite size effect (eV)	Relativistic recoil effect (eV)	Strong interaction effect (eV)	Total energy (eV)
$3p$	-14685.15	-11.56	-0.08	$+0.01$	-0.02	-0.78	-14697.58
$3d$	-14682.65	-5.39	-0.04	$+0.0005$	-0.02	$< 10^{-4}$	-14688.10
$4d$	-8259.04	-2.10	-0.02	$+0.0003$	-0.01	$< 10^{-4}$	-8261.17
$4f$	-8258.59	-0.72	-0.004	$+0.0003$	-0.01	$< 10^{-4}$	-8259.32

Transitions	Electron screening effect (eV) Configuration	K-shell contribution	L-shell contribution	Transition energy (eV)
$4f \rightarrow 3d$	no electron	—	—	6428.78
	$1s^1\,2s^2\,2p^1$	-0.19	-0.02	6428.57
	$1s^2\,2s^2\,2p^1$	-0.31	-0.01	6428.46
		Experimental result (this work):		$6428.39 \pm 0.13 \pm 0.09$
$4d \rightarrow 3p$	no electron	—	—	6436.41
	$1s^1\,2s^2\,2p^1$	-0.25	-0.02	6436.14
	$1s^2\,2s^2\,2p^1$	-0.42	-0.01	6435.98
		Experimental result (this work):		$6435.76 \pm 0.30\,^{+0.11}_{-0.07}$

$$I(4d \rightarrow 3p)/I(4f \rightarrow 3d) = 0.30 \pm 0.03(\text{stat.}) \pm 0.02(\text{syst.}),$$

where the first error is statistical and the second is systematic. The quoted systematic uncertainty is a quadratic summation of the contributions from uncertainties in the energy calibration, the non-Gaussian response function, and the timing window width. The tail component of the Fe K_α line affects the fit results. We assessed it by varying the relative strength of the Fe X-ray tail by changing the timing window. The Fe tail is the main source of systematic errors both for X-ray energies and yield ratio. The energy dependence of transmissions of these two π-^{12}C peaks is negligible in determining the yield ratio, since these energies are very close and no absorption edge structure exists around those peaks.

We have calculated the $3p$, $3d$, $4d$, and $4f$ energy levels of the pionic ^{12}C using only the electromagnetic (EM) interaction and tabulated the results in Table 1. These EM values are calculated from the Klein–Gordon equation including vacuum polarization with higher-order correction, the relativistic recoil effect, and the nuclear finite size effect. The latest charged pion mass, 139.57018(35) MeV/c^2, given by the Particle Data Group [29] is used.

Strong interaction effects on these energy levels were assessed via the Seki–Masutani potential [30]. The strong interaction shift of the $3p$ level from its EM value is calculated to be 0.78 eV, while the shifts of the $4f$, $4d$, and $3d$ levels are below 10^{-4} eV.

The effect of the electrons populating the K- and L-shells, the so-called electron screening effect, is not negligible, especially in the solid target. The electron screening correction to the X-ray energy is

largely determined by the number of $1s$ electrons in the atom, which depends on the balance between Auger electron emission and the electron refilling process from neighboring atoms. We have estimated the electron screening effect with the "$Z-1$" approximation, namely the captured pion screens one unit of the nuclear charge seen by the electrons. Thus, the maximum electron screening correction is given by the $1s^2\,2s^2\,2p^1$ electronic configuration. In Table 1, the EM values of the $4f \rightarrow 3d$ and $4d \rightarrow 3p$ transitions are tabulated for the no electron, $1s^1\,2s^2\,2p^1$, and $1s^2\,2s^2\,2p^1$ electronic configurations. Here, the electron density functions in each configuration are evaluated using the hydrogenic wave function with effective nuclear charge based on Hartree–Fock calculations. The experimental results are consistent with the $1s^2\,2s^2\,2p^1$ configuration within the errors.

4. *Conclusion* We observed the π-^{12}C $4f \rightarrow 3d$ transition X-ray line with a novel 240 pixel microcalorimetric X-ray detector based on transition-edge sensors. The achieved averaged energy resolution is 6.8 eV FWHM at 6.4 keV under a high-rate pion beam intensity of 1.45 MHz. The timing resolution is 1.2 μsec FWHM. Absolute energy calibration is realized by an X-ray generator shining on calibration metals during the data acquisition. The resulting systematic uncertainty in the π-^{12}C $4f \rightarrow 3d$ transition X-ray energy is less than 0.1 eV, which meets our goal for a future measurement of the kaonic helium $3d \rightarrow 2p$ X-ray energy.

The TES spectrometer had sufficient energy resolution to observe the parallel transition π-^{12}C $4d \rightarrow 3p$ X-ray for the first time. The strong interaction effect of the $3p$ level is not negligible because it has smaller angular momentum than the $3d$ level. The measured X-ray energy of the parallel transition $4d \rightarrow 3p$ was found to be consistent with the calculated strong interaction effect assessed via the Seki–Masutani potential [30].

Our data allow the determination of the electron population status of the atoms. Both the $4f \rightarrow 3d$ and $4d \rightarrow 3p$ transition energies obtained favor two $1s$ electrons in the K-shell. Moreover, we have determined the yield ratio between the $4f \rightarrow 3d$ and $4d \rightarrow 3p$ transitions. Whether the observed X-ray yields can be consistently explained by a cascade calculation with the electronic configuration of two filled $1s$ electrons in the K-shell remains to be solved in future theoretical work.

We successfully demonstrated the feasibility of hadronic atom X-ray spectroscopy with an absolute energy uncertainty of 0.1 eV in the 6 keV energy region. This is an important milestone towards a more general use of high-resolution microcalorimeter spectrometers at charged particle beamlines.

Acknowledgements

The authors thank K. Deiters and the PSI staff for beamline coordination and operation. J. Uhlig thanks the Knut and Alice Wallenberg Foundation for their continued support. This work was partly supported by RIKEN, NIST, KEK, Grants-in-Aid for Scientific Research from MEXT and JSPS (Nos. 25105514, 26707014, 24105003, 15H05438, and 15H00785), the Strategic Young Researcher Overseas Visits Program for Accelerating Brain Circulation by JSPS (No. R2509), Incentive Research Grant from RIKEN, Mitsubishi Foundation (26145), and the NIST Innovations in Measurement Science Program.

References

[1] M. Bazzi et al. [SIDDHARTA Collaboration], Phys. Lett. B **704**, 113 (2011).
[2] M. Bazzi et al. [SIDDHARTA Collaboration], Nucl. Phys. A **881**, 88 (2012).
[3] Y. Ikeda, T. Hyodo, and W. Weise, Phys. Lett. B **706**, 63 (2011).
[4] Y. Ikeda, T. Hyodo, and W. Weise, Nucl. Phys. A **881**, 98 (2012).
[5] A. Gal, Nucl. Phys. A **914**, 270 (2013).
[6] S. Okada et al., Phys. Lett. B **653**, 387 (2007).
[7] M. Bazzi et al. [SIDDHARTA Collaboration], Phys. Lett. B **697**, 199 (2011).

[8] M. Bazzi et al. [SIDDHARTA Collaboration], Phys. Lett. B **681**, 310 (2009).
[9] S. Baird, C. J. Batty, F. M. Russell, P. Sharman, P. M. Bird, A. S. Clough, K. R. Parker, G. J. Pyle, and G. T. A. Squier, Nucl. Phys. A **392**, 297 (1983).
[10] Y. Akaishi, Proc. Int. Conf. on Exotic Atoms (EXA05), 45 (2005).
[11] S. Hirenzaki, Y. Okumura, H. Toki, E. Oset, and A. Ramos, Phys. Rev. C **61**, 055205 (2000).
[12] C. J. Batty, Nucl. Phys. A **508**, 89c (1990).
[13] E. Friedman, Hyperfine Interact. **209**, 127 (2011).
[14] K. Agari et al., Prog. Theor. Exp. Phys. **2012**, 02B011 (2012).
[15] R. S. Hayano et al., *Proposal for J-PARC 30 GeV Proton Synchrotron: Precision Spectroscopy of Kaonic Atom X-rays with TES*, J-PARC E62 (2015).
[16] S. J. Smith, J. S. Adams, C. N. Bailey, S. R. Bandler, J. A. Chervenak, M. E. Eckart, F. M. Finkbeiner, R. L. Kelley, C. A. Kilbourne, F. S. Porter, and J. E. Sadleir, J. Low. Temp. Phys. **167**, 168 (2012).
[17] J. Uhlig et al., J. Synchrotron Radiat. **22**, 766 (2015).
[18] K. D. Irwin and G. C. Hilton, Transition-Edge Sensors. In *Cryogenic Particle Detection*, Topics in Applied Physics, vol. 99, ed. C. Enss (Springer, New York, 2005).
[19] J. N. Ullom and D. A. Bennett, Supercond. Sci. Technol. **28**, 084003 (2015).
[20] D. Gotta et al., Lect. Notes Phys. **745**, 165 (2008).
[21] M. Trassinelli et al., Phys. Lett. B, **759**, 583 (2016).
[22] K. Deiters. *piM1 beam line* (Paul Scherrer Institut, Villigen, Switzerland). (Available at: http://aea.web.psi.ch/beam2lines/beam_pim1.html, date last accessed August 25, 2016).
[23] J. N. Ullom, W. B. Doriese, D. A. Fischer, J. W. Fowler, G. C. Hilton, C. Jaye, C. D. Reintsema, D. S. Swetz, and D. R. Schmidt, Synchrotron Radiat. News **27**, 24 (2014).
[24] High Precision Devices, Inc. *Cryostat Model 102 Denali* (HPD, Boulder, CO). (Available at: http://www.hpd-online.com, date last accessed August 25, 2016).
[25] W. B. Doriese et al., J. Low. Temp. Phys. **184**, 389 (2016).
[26] J. W. Fowler, B. K. Alpert, W. B. Doriese, Y.I. Joe, G. C. O'Neill, J. N. Ullom, and D. S. Swetz, J. Low. Temp. Phys. **184**, 374 (2016).
[27] G. Hölzer, M. Fritsch, M. Deutsch, J. Härtwig, and E. Förster, Phys. Rev. A **56**, 4554 (1997).
[28] H. Tatsuno et al., J. Low. Temp. Phys. **184**, 930 (2016).
[29] K. A. Olive et al. [Particle Data Group], Chin. Phys. C **38**, 090001 (2014).
[30] R. Seki and K. Masutani, Phys. Rev. C **27**, 2799 (1983).